Optical Excitations in Carbon Architectures Based on Dodecadehydrotribenzo[18]annulene†

Smriti Anand,‡,⊥ Oleg Varnavski,§ Jeremiah A. Marsden,|| Michael M. Haley,|| H. Bernhard Schlegel,‡ and Theodore Goodson, III*,§

Department of Chemistry and Institute for Scientific Computing, Wayne State University, Detroit, Michigan 48202, Department of Chemistry, University of Michigan, Ann Arbor, Michigan 48109, and Department of Chemistry and Material Science Institute, University of Oregon, Eugene, Oregon 97403

Received: July 18, 2005

The origin of excitations in multi-chromophore carbon network substructures based on dodecadehydrotribenzo[18]annulene has been investigated by steady-state and photon echo spectroscopy, configuration interaction (CIS and CIS(D)), and time-dependent density functional theory (TD-DFT). 1,4-Diphenylbutadiyne, the simplest structural subunit within the annulene, was used in modeling the spectroscopic studies to explain the origin of excitations in the macrocycles. The optical excitations in longer linear systems were found to be similar to its diphenylacetylene analogue. However, the results from dodecadehydrotribenzo[18]annulene and other multichromophore networks systems illustrate the possibility of strong intramolecular interactions and the formation of delocalized excited states. Calculations were carried out to explain the basic similarities and differences in excitations of the model compounds such as diphenylbutadiyne and the macrocycles. The fundamental excitation in these systems can be primarily described as a $\pi \rightarrow \pi^*$ transition. Two low-energy resonances were observed from experiment for the annulene systems, and possible explanations for these low-energy resonances in the macrocycles are explored. The significant difference found in the calculated oscillator strength of the two low-energy bands for the macrocycles as well as the dynamics of solvent interactions was further investigated by three-pulse photon echo measurements. A simple exciton model was developed to discuss the excitations in the larger macrocycles. The results from this model were found to be in good agreement with the TD-DFT calculations.

Introduction

The optical applications of multi-chromophore macromolecules such as conjugated polymers and oligomers,[1] rotaxanes,[2] and dendrimers[3] have attracted great interest because of the possibility for these structures to display enhanced optical effects attributable to the strongly interacting multi-chromophore geometry.[3] Many of these systems are synthesized (fabricated) in a self-similar fashion with conjugated chromophores as building blocks.[4] In the case of dendrimers, for example, the building blocks can be used to form a fractal or branched macromolecular geometry, which increases in size with generation.[4−6] Previous reports have investigated the nature of excitations in such systems and observed the characteristics of coherent energy migration in some cases.[7] These findings imply that there can be a large number of interacting chromophores participating in the energy transport. While this property certainly precludes possible applications in linear and nonlinear optics, by virtue of enhancing the transition dipole moment,[8] investigations with these and other related macromolecules may also result in an improved understanding of the mechanism of energy transport in multi-chromophore architectures.

As mimics of the all-carbon architecture graphdiyne (GR),[9] a series[10,11] of multi-chromophore systems based on dodecadehydrotribenzo[18]annulene (triangle, TR)[12,13] has been prepared. The interest in this and other macromolecular carbon networks arises from predictions of useful properties such as conductivity and nonlinear optical activity.[9,14−17] It has been suggested that these enhanced properties are the result of their beneficial multi-chromophore-ordered structure (geometry). The absorption spectrum of these macrocycles[10] showed four diagnostic peaks, with two low intensity peaks appearing at longer wavelength than the most intense peak. When two of the [18] annulenes were fused together, the low-energy peaks showed a red-shift and an increase in intensity.

Calculations of the optimized geometry and electronic band structures of GR and related carbon allotropes were carried out using periodic boundary conditions with the local spin-density approximation.[15−17] It was found that the hexagons in such architectures are equilateral and all bond angles are either 120° or 180°. The bond length of a hexagon in these carbon allotropes is almost equal to that of graphite and is somewhat longer than the bond that links the hexagon to the outside carbon. This gives an insight into the geometry of the newly developed architectures as it has been shown that the geometry has a strong effect on the optical excitations.[18] Measurements of the molecular hyperpolarizability (β) of macrocycles, based on TR, functionalized with electron donor and acceptors groups have shown that these interesting systems might give rise to promising nonlinear optical effects that vary with the molecular geometry.[19]

† Part of the special issue "William Hase Festschrift".

* To whom correspondence should be addressed. E-mail: tgoodson@umich.edu.

‡ Wayne State University.

⊥ Current address: Christopher Newport University, Newport News, VA 23606.

§ University of Michigan.

|| University of Oregon.

10.1021/jp0539573 CCC: $33.50
Published on Web 09/24/2005

SCHEME 1: Structures of the Molecules Studied

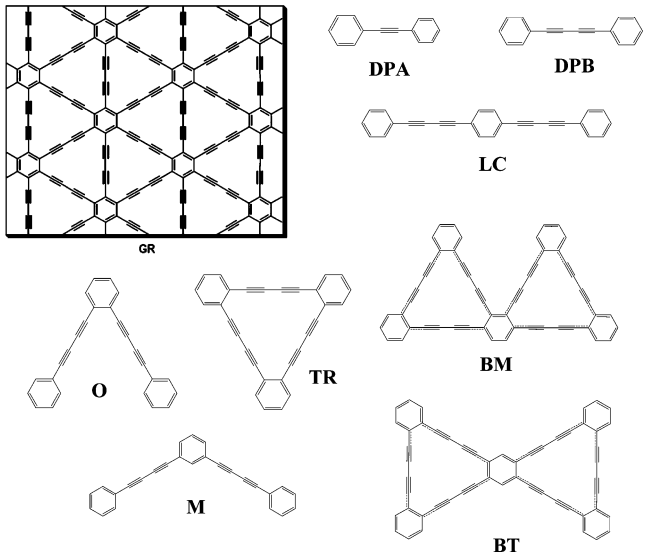

Both the network substructures and the functionalized TR macrocycles investigated in this report are comprised of multiple 1,4-diphenylbutadiyne (DPB) chromophores, the basic building block that is interconnected by linkages of the phenyl rings (see Scheme 1). The steady-state and time-resolved optical excitations of DPB and similar analogues have been reported in the literature.[20,21] Hoshi et al.[20] have investigated the polarized absorption spectrum of DPB probed in a stretched polyethylene film. It was found that the 30 250 and 38 020 cm^{-1} electronic bands are polarized along the long axis of the molecule. The 30 250 cm^{-1} band was assigned to a $\pi \rightarrow \pi^*$ ($S_0 \rightarrow S_1$) transition, and the 38 020 cm^{-1} band was assigned to a $\pi' \rightarrow \pi'^*$ ($S_0 \rightarrow S_6$) transition. They have also carried out theoretical calculations on DPB and other diphenylpolyynes using the Pariser−Parr−Pople (PPP) method. The excitation has been explained in terms of the molecular orbital (MO) and transition densities of the phenyl and polyyne moieties. There have been reports of the dynamics of electronic transitions in related molecular systems as well.[21] In several cases, transient absorption was used to probe these processes due to the fact that DPB has a relatively low fluorescence quantum yield (much less than 1×10^{-3} in cyclohexane) at room temperature.[21]

Hirata and co-workers[21] have used ultrafast transient absorption spectroscopy to probe the dynamical behavior of the S_2 state of DPB and its methoxy derivatives in solution. From the transient absorption data, it was deduced that the major part of the first absorption band does not correspond to a $S_0 \rightarrow S_1$ transition. If this had been so, then the transition moment between these states should have been significantly smaller than that of the first absorption band observed. This is similar to the case of diphenylacetylene (DPA, see Scheme 1)[22] where the S_1 state was found to be nonfluorescent and the first observed absorption band was assigned to the $S_0 \rightarrow S_2$ ($^1B_{1u}$) transition. Studies by Ferrante et al.[23] have shown that $^1B_{1u}$ is the lowest singlet excited state at the ground-state equilibrium geometry and is responsible for the fluorescence spectrum and the lowest energy absorption band of DPA. But for longer C≡C bonds, a state with A_u symmetry is calculated to be the lowest in energy. These two states can be considered as excited-state isomers, and since the A_u state is the lowest state at its own equilibrium geometry, the fluorescing state was assigned as S_2 by Hirata et al.[22] Karabunarliev et al.[24] studied the *p*-phenylene ethynylene [$(PE)_n$, $n = 2-6$] systems using the AM1-CAS-CI method and found the ^1B_u state to be the lowest one-photon excited state. Their studies also showed that the largest amplitude of the exciton resided on the bridgehead phenyl/phenylene site in these systems and suggested a delocalization of the excited state. Marder and co-workers[25] investigated the photophysical properties of 1,4-bis(phenylethynyl) benzene at 283 K and found no evidence for aggregation in the concentration range $1-250 \times 10^{-6}$ mol dm^{-3}. However, in a viscous low-temperature glass, some changes were observed in the absorption and emission spectra. Sluch et al.[26] studied the absorption and emission spectra of the oligo(phenylene ethylene) nonamer. Their results suggest that a partial planarization occurs more quickly than what could be detected with the time resolution of the experiment.These results, in general (steady-state and time-resolved), show that the rate of relaxation is directly connected to the solvent viscosity or that the relevant motions must displace a significant amount of solvent, and this is related to torsional motion.[26] Levitus et al.[27] carried out photophysical measurements on 1,4-bis(phenylethynyl)benzene to study the effects of phenyl rotation and chromophore aggregation. The shift of 10−20 nm with high vibrational resolution was attributed to planarization while aggregation of the chromophores gave larger shifts of about 70 nm.

Perhaps the most general comment which could be made in regards to these structures is that important parameters such as geometric disorder and electronic interactions play a major role in both the differences in steady-state and time-resolved phenomena observed in the various annulene and bis-annulene systems. Further information then concerning the electronic structure (to a high level of theory), characterization of site-to-site disorder of the excitation energies, and the process of electron−phonon coupling will add to the understanding of distinguishing characteristics of these systems. The process of geometrical distortions as well as solvent (bath) interactions may also play a large role in this discussion. In many multi-chromophore systems, such as those described in the present report, the issue of dephasing may also contribute to the changes observed in the electronic properties of the macromolecular structures in comparison to their linear molecular analogues. The mechanisms that give rise to a relatively broadened spectrum for the organic systems studied here may involve ultrafast transient phenomena, which are related to the effects of dephasing and inhomogeneous broadening. Different methods have been used to probe these fast processes in solution with great success. One such technique is the three-pulse photon echo peak shift (3PEPS) method.[28,29] This technique has already been thoroughly applied to the natural light harvesting system and in semiconducting nanoparticles,[30] and it is also applied to the present systems studied in this contribution. The purpose of the photon echo measurements is to estimate (qualitatively) the extent of coupling to the bath and the long-range delocalization in these multi-chromophore systems as well as different oscillator strengths of individual bands. Comparison to the calculated value is also provided.

To explain the excitations in the annulene and bis-annulene systems, investigations of electronic spectroscopy and electronic structure theory calculations are used to correlate the structure/property relationships. Time-resolved nonlinear spectroscopy is also used to probe the degree of interaction between the participating chromophores and to experimentally examine the strengths of various transitions (in particular, the two low-energy bands) in the macrocycles. The molecules studied are diphenylacetylene (DPA), diphenylbutadiyne (DPB), 1,2-bis(phenylbutadiynyl)benzene (ortho, O), 1,3-bis(phenylbutadiynyl)-benzene (meta, M), 1,4-bis(phenylbutadiynyl)benzene (long

chain, LC), dodecadehydrotribenzo[18]annulene (triangle, TR), and the two bis-annulenes (boomerang, BM, and bowtie, BT). These investigations provide new insight into the distinguishing characteristics of multi-chromophore macromolecules built on the bis-annulene framework.

Experimental Methods

Sample Preparation. 1,4-Diphenylbutadiyne (DPB) was purchased from Aldrich, and its purity was 99%. Macrocycles TR and BM were prepared and purified as reported in the literature.[10] 1,4-Bis(phenylbutadiynyl)benzene (LC) was synthesized in 87% yield from 1,4-diiodobenzene and (4-phenylbutadiynyl)triisopropylsilane[31] via sequential desilylation/alkynylation (see Supporting Information for experimental details). Recrystallization from benzene gave LC, a tan solid, whose spectral and physical properties matched those previously reported.[31] Solutions of the diacetylenic molecules were prepared in spectral grade $CHCl_3$ at concentrations of 2.0×10^{-4} M for absorption measurements.

Steady-State Measurements. Linear absorption measurements were performed on a Hewlett-Packard 8452A diode array spectrophotometer. The sample cell was placed at an incident angle of ca. 45°, and the fluorescence was collected at 90° to the incident laser beam using fiber optical cable interfaced to a spectrometer.

Three-Pulse Photon Echo Studies. Three-pulse photon echo experiments were carried out with a cavity-dumped Kerr lens mode-locked Ti-sapphire laser pumped by a frequency-doubled YVO laser (Millennia, Spectra Physics). The cavity-dumper efficiency was about 30%. The cavity-dumped laser pulse had a duration of 19 fs. The pulse spectrum was centered at ~834 nm. The cavity-dumped beam was focused into a 0.5 mm BBO crystal to convert the fundamental beam into the second harmonic at ~415 nm. Unless mentioned otherwise, the pulse repetition rate was fixed at 77 kHz.

In the 3PEPS experiment,[28,29,32] both echo signals at phase-matching conditions $k_1 - k_2 + k_3$ and $-k_1 + k_2 + k_3$ are simultaneously recorded while the time period τ between pulses 1 and 2 is scanned. Half of the distance between the intensity peaks of these two signals is called "peak shift", which is the essential quantity deduced from the experiment. Thus, the echo peak shift is obtained from the echo profiles and then recorded as a function of population period T between the second and the third pulse. The third pulse creates the superposition state, which may lead, in case of a proper phase evolution, to the photon echo formation.[28,29] Photon echo peak shift is sensitive to the extent of the correlation of the phase evolution between the first and the second coherence periods, which is, in turn, sensitive to the transition frequency dynamics during the population period. In our setup, three beams of equal intensities (~0.5 nJ per pulse in one beam at the sample) were generated with the aid of thin beam splitters (1 mm thick quartz substrate, CDP).[33] One pulse (k_1) traveled a fixed delay whereas the other two pulses (k_2 and k_3) traveled variable delays formed with retroreflectors mounted on DC motor-driven delay stages (Newport ILS100CCHA) controlled via a Newport ESP7000 motion controller. The three beams were aligned after the delay stages to form the equilateral triangle beam geometry (8 mm sides) and were focused into the 440 mm quartz sample cell using thin singlet lens ($f = 18$ cm). The two third-order nonlinear signals into the $k_1 - k_2 + k_3$ and $-k_1 + k_2 + k_3$ phase matching directions were spatially filtered and directed to two photomultipliers (Hamamatsu Photo Sensor Modules H6780). The electrical signals from photomultipliers were measured by two lock-in amplifiers (Stanford Research, SR830), which were referenced to the chopper (SR540) inserted in the k_1 beam. Many measurements were performed in order to confirm reproducibility of the signal.[33] Special attention was paid to the residual peak shift value. The uncertainties of the peak shift value can be estimated at approximately ±0.5 fs over the entire population period up to 100 ps.[33]

Theoretical Methods

All electronic structure calculations were carried out using the Gaussian[34] suite of programs. The ground-state molecules were optimized by semiempirical [AM1], Hartree−Fock [HF/3-21G], and density functional methods[35,36] [B3LYP/3-21+G and B3LYP/6-31+G(d)]. The excited states in these systems were studied by the configuration interaction with single excitation (CIS),[37] with perturbative correction for double excitations (CIS(D))[38,39] and time-dependent density functional theory[40−42] with the B3LYP functional (TD-B3LYP) with the STO-3G, 3-21+G and 6-31+G(d) basis sets. Diffuse and polarization functions were included to describe the excited state in a better fashion. This should provide good agreement for trends in the excitation energies. However, larger basis sets and higher levels of theory are needed to obtain more accurate excitation energies. The CIS(D) and TD-DFT methods were used to calculate the vertical excitation energies and oscillator strengths of the molecules in this study since they provide a considerable improvement over CIS, even for small systems such as benzene.[42]

A transition from the ground-state ψ_g to an excited state ψ_e is dipole allowed if the integral $\mu_{ge} = \langle \psi_g | \hat{\mu} | \psi_e \rangle$ is non zero, where $\hat{\mu}$ is the dipole moment operator.[43] As is well-known from group theory, the transition $\psi_g \leftrightarrow \psi_e$ will be dipole allowed only if the direct triple product $\Gamma_g \times \Gamma_{\hat{\mu}} \times \Gamma_e$ contains the totally symmetric representation; all other transitions are dipole forbidden. The intensity of the transition is determined by the oscillator strength, which is proportional to the square of the transition dipole moment:

$$f_{ge} = \frac{2m\omega_{ge}|\mu_{ge}|^2}{3e^2\hbar} \tag{1}$$

where $\omega_{ge} = 2\pi\nu_{ge}$ is the transition frequency.

A series of vibrational transitions within an electronic transition leads to a Franck−Condon (FC) progression, and the difference in bond lengths between the electronic states governs the intensity distribution within this progression. The FC factor is given by the square of the overlap of the initial and final vibrational states. For a transition from $v'' = 0$ in the ground electronic state to vibrational level v' in the excited electronic state, the FC factor is[43]

$$F_{ov} = |\langle 0^g | v^e \rangle|^2 = \frac{1}{v!}\left(\frac{\Delta^2}{2}\right)^v \exp(-\Delta^2/2) \tag{2}$$

where the vibrational frequency and normal modes are assumed to be the same in the ground and excited states. The dimensionless normal mode displacement Δ is given by

$$\Delta \equiv \left(\frac{\omega_i}{m_i\hbar}\right)^{1/2}(x_{0i}^e - x_{0i}^g) \tag{3}$$

where x_{0i}^g and x_{0i}^e are the equilibrium values of the ith normal mode in the ground and excited state, respectively, and m_i is the reduced mass.

Transitions that are forbidden by the dipole selection rules can gain intensity by vibronic coupling, if there are vibrations

of an appropriate symmetry that can couple the two electronic states. One approach to compute the vibronic coupling is to examine the coordinate dependence of the transition dipole moment:[43]

$$\mu_{ge} = \mu_{ge}^{0} + \sum_{i=1}^{3N-6}\left(\frac{\partial \mu_{ge}}{\partial x_i}\right)_0 x_i + ... \quad (4)$$

Here, the term $(\partial\mu_{ge}/\partial x_i)$ connects the states ψ_g and ψ_e if the product $\Gamma_g \times \Gamma_{\hat{\mu}} \times \Gamma_e \times \Gamma_{x_i}$ contains the totally symmetric representation. When $\mu_{ge} = 0$, the oscillator strength due to vibronic coupling with mode i is given by

$$f_{ge}^{vib} = \frac{2m\omega_{ge}\left(\frac{\partial \mu_{ge}}{\partial x_i}\right)^2 \langle 0^g|x_i|v^e\rangle^2}{3e^2\hbar} \quad (5)$$

This approach has been used to study the vibronic activity in benzene[44] and is employed here. In the present study, the triangle molecule (TR) was displaced by 0.2 Å along suitable normal modes, and the transition dipole moment was recalculated. The vibronic contributions to the oscillator strength were computed from the squares of the numerical derivative of the transition dipole moment and the appropriate harmonic oscillator (HO) matrix elements and the Franck−Condon factors for the remaining modes. The HO matrix elements are

$$\langle 0^g|x_i|v^e\rangle^2 = \left(\frac{\hbar}{2m\omega_i}\right)\left(\frac{1}{v!}\right)\left(\frac{\Delta^2}{2}\right)^{v-1}\left(v - \frac{\Delta^2}{2}\right)^2 \exp(-\Delta^2/2) \quad (6)$$

where Δ is the dimensionless normal mode displacement represented by eq 3.

Zero point vibration (ZPE) and thermal excitation of low-frequency modes of the ground-state vibrations may also contribute to the intensity of an electronic transition. The ZPE contribution to the oscillator strength is given by

$$f^{eff} = f + \sum_i \frac{\partial^2 f}{\partial x_i^2}\langle 0|x_i^2|0\rangle + ...$$

$$= f + \sum_i \frac{\partial^2 f}{\partial x_i^2}\frac{\hbar}{2m\omega_i} + ... \quad (7)$$

and the thermally averaged contribution is given by

$$f^{eff} = f + \sum_i \frac{\partial^2 f}{\partial x_i^2}\sum_v \langle v|x_i^2|v\rangle \exp\left(\frac{-\hbar\omega_i(v + 1/2)}{kT}\right)$$

$$f^{eff} = f + \sum_i \frac{\partial^2 f}{\partial x_i^2}\left(\frac{\hbar}{2m\omega_i} + \frac{\hbar/m\omega_i}{\exp(\hbar\omega_i/kT) - 1}\right) \quad (8)$$

where $\langle v|x_i^2|v\rangle = \hbar/m\omega_i\,(v + 1/2)$. If higher terms in eq 4 are ignored, the second derivative of the oscillator strength can be obtained by substituting eq 4 into eq 1:

$$\frac{\partial^2 f}{\partial x_i^2} = \frac{2m\omega_{ge}\left(\frac{\partial \mu_{ge}}{\partial x}\right)^2}{3e^2\hbar} \quad (9)$$

Results and Discussion

Structure and Symmetry from Electronic Structure Theory Calculations. All the molecules studied have a planar geometry in the equilibrium ground state. The linear systems DPA, DPB, and LC belong to the D_{2h} point group; the triangle molecule (TR) is of D_{3h} symmetry; boomerang (BM) has C_{2v} symmetry; and the bowtie (BT) has D_{2h} symmetry. The ground state for the linear molecules and BT is ^1A_g while the ground state of TR is $^1A'$ and that of BM is $^1A_1$. The C≡C bond lengths are all in the range of ∼1.19−1.22 Å, and the C≡C symmetric stretching frequencies are approximately 2200−2400 cm^{-1}. For a given level of theory, all of the C≡C bond lengths are within ±0.003 Å of each other, and the C≡C symmetric stretching frequencies are within ±30 cm^{-1} of each other. At the HF/3-21G level of theory, the optimized conformers with the phenyl rings constrained to be perpendicular to each other were 0.42 and 0.06 kcal/mol higher than the planar conformer in DPA and DPB, respectively. In both the systems, the single imaginary frequency present in the twisted structures corresponds to the rotation of the phenyl rings. In LC, the structure with only one of the terminal phenyl rings perpendicular to the rest of the molecule was only 0.08 kcal/mol higher in energy than the totally planar structure. With both the phenyl rings perpendicular to the central ring, the optimized structure was about 0.17 kcal/mol higher in energy than the planar conformation. This structure had two imaginary frequencies corresponding to the rotation of the two terminal rings. The energies of the twisted conformers in all the linear systems are less than the thermal energy (kT) at room temperature, and thus the terminal phenyl rings behave as free rotors. This might lead to the broadening of the absorption spectrum as in the ground state the various rotomers are equally probable. By contrast, the triangle molecule has no rotatable groups. However, there are six normal modes with frequencies of less than 100 cm^{-1} that correspond to the out-of-plane motion of the molecule. Thus, the triangle molecule has considerable flexibility even though its connectivity prevents any free rotation.

The first excited state was optimized within D_{2h} symmetry for DPA, DPB, and LC using the CIS and TD-DFT methods. The excited states correspond to a $\pi \rightarrow \pi^*$ transition of ^1B_u symmetry and the molecules remain planar. The ground- and excited-state geometry and frequencies for DPA and DPB are compared in Table 1. The main geometric changes are a lengthening of the C≡C bond by 0.04−0.06 Å and a shortening of the adjacent C−C single bonds by 0.04−0.07 Å. This is accompanied by a red-shift of the C≡C symmetric stretching frequencies of 150−250 cm^{-1}. The phenyl C−C bonds closest to the acetylenic π system change by ∼ +0.02 to +0.04 Å in the excited state. In the central phenyl ring of LC, the C−C bonds parallel to the long axis shorten by ∼0.02 Å, resulting in a quinoidal distortion. The changes are much smaller for the remaining C−C bonds in the phenyl rings of the other structures. Excited-state calculations at CIS/3-21G, TD-B3LYP/STO-3G, and TD-B3LYP/3-21+G show very similar changes in geometry. The twisted conformers of the excited states of DPA and DPB were also optimized. The rotational barrier in the excited state is 15.2 kcal for DPA and 1.6 kcal/mol for DPB at the CIS/3-21G level of theory. A similar increase in rotational barriers in the excited state has been noticed for 1,4-bis-(phenylethynyl)benzene[27] and in other phenylene-based conjugated oligomers.[24]

The first three excited states of the TR molecule were optimized using the TD-DFT/STO-3G and TD-DFT/3-21+G methods, and the changes are presented in Table 1. The details of the excited states arising due to a transition from the highest occupies molecular orbital (HOMO) to the lowest unoccupied molecular orbital (LUMO) are discussed later in the text. The

TABLE 1: Comparison of Calculated Ground and Excited State C≡C Bond Length and Scaled Vibrational Frequencies in DPA, DPB, and TR[a,b]

	C≡C	C−C	C−Ph	frequency[b]
		DPA		
ground state				
HF/3-21G	1.192		1.432	2305.7
B3LYP/STO-3G	1.215		1.452	2259.2
B3LYP/3-21+G	1.216		1.425	2226.5
excited state				
CIS/3-21G	1.247		1.371	2049.6
TD-B3LYP/STO-3G	1.259		1.402	2063.3
TD-B3LYP/3-21+G	1.253		1.378	2077.6
		DPB		
ground state				
HF/3-21G	1.193	1.368	1.431	2363.1
B3LYP/STO-3G	1.222	1.384	1.449	2246.7
B3LYP/3-21+G	1.221	1.354	1.422	2248.9
excited state				
CIS/3-21G	1.249	1.301	1.394	2164.8
TD-B3LYP/STO-3G	1.282	1.312	1.409	2097.6
TD-B3LYP/3-21+G	1.259	1.311	1.384	2112.2
		TR		
ground state				
HF/STO-3G	1.180	1.401	1.453	2337.3
HF/3-21G	1.192	1.367	1.427	2498.2
B3LYP/STO-3G	1.223	1.382	1.445	2214.6
B3LYP/3-21G	1.219	1.349	1.414	2235.3
A'_2 excited state				
CIS/STO-3G	1.197	1.371	1.427	2215.5
TD-B3LYP/STO-3G	1.238	1.360	1.421	2163.2
A'_1 excited state				
CIS/ STO-3G	1.185	1.391	1.438	2186.1
TD-B3LYP/STO-3G	1.239	1.357	1.417	2126.8
E′ excited state[c]				
CIS/ STO-3G	1.206	1.355	1.437	1953.8
	1.181	1.399	1.449	1921.0
TD-B3LYP/STO-3G	1.236	1.362	1.432	2063.1
	1.234	1.368	1.431	2183.2

[a] Bond lengths in Å, and scaled frequencies in cm^{-1} (scale factor: 0.827 for HF/STO-3G and CIS/STO-3G, 0.9085 for HF/3-21G and CIS/3-21G, 0.9156 for B3LYP/STO-3G and TD-B3LYP/STO-3G, and 0.9614 for B3LYP/3-21+G and TD-B3LYP/3-21+G). [b] The symmetric C≡C stretching mode. [c] E′ state is of C_{2v} symmetry.

two A states retain the D_{3h} symmetry and the E state optimized to C_{2v} symmetry. The changes in the bond lengths and vibrational frequencies show the same trends observed in DPA and DPB but are significantly smaller.

Steady-State Measurements. The absorption spectra of compounds DPB, LC, and TR are depicted in Figure 1a, and that of TR, LC, BM, and BT are depicted in Figure 1b. DPB has a major peak at 330 nm, which corresponds to the ^1A_g to $^1B_{1u}$ transition.[20,22] The other peaks are attributed to the vibrational progression of carbon triple bonds[7] and twisting of the end phenyl rings. The "long chain" molecule (LC), which is an extended version of DPB, displays a red-shift of ca. 30 nm in the absorption spectra and a low-energy peak at 360 nm. The differences in the absorption spectra of structure DPB → LC are similar to the differences observed in comparing diphenylacetylene to 1,4-bis(phenylethynyl)benzene.[27] The absorption spectrum of LC shows several vibronic features that are overlapped and are not as clear as those seen in DPB. This may be due to the fact that LC is more flexible than DPB.

Comparison of the spectra in Figure 1 may allow some of the features to be rationalized on a phenomenological basis. Although the principal absorption band in TR is similar to that of DPB at 330 nm, there are two additional peaks at longer wavelengths (360 and 370 nm) with extinction coefficients on the order of $\sim 5 \times 10^4$ mol^{-1} cm^{-1}. On the basis of the linear

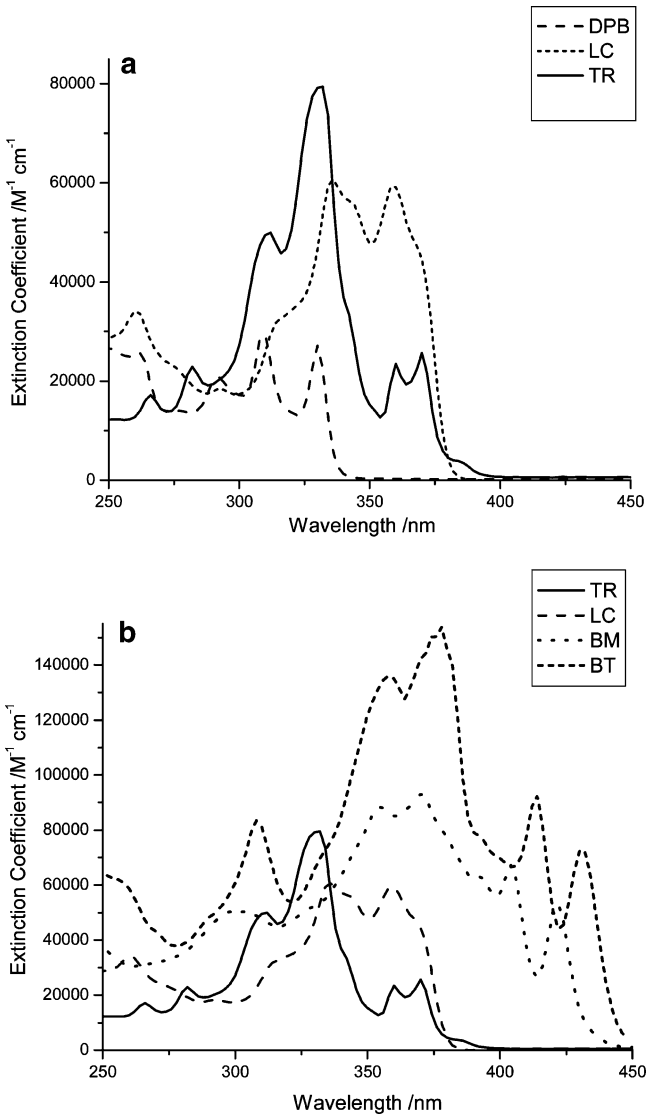

Figure 1. Comparison of the absorption spectra of (a) DPB, LC, and TR and (b) TR, LC, BM, and BT.

absorption spectra for the two systems (DPB and TR), it would appear that their excitations are similar (apart from the two additional peaks in the TR molecule at lower energy). The identity of the low-energy peaks was examined by time-resolved experiments as well as through calculations (see below). However, the other features of the absorption spectra of DPB and TR are very similar. This may suggest that the excitations are localized on one (or two) of the linear chromophores in the TR molecule. This hypothesis can be tested by examining the electronic structure calculations. Furthermore, the origin of the two additional peaks at lower wavelength may be attributable to delocalized excitonic interactions of the sides of TR. Again, the calculations can be used to test this possibility. Boomerang (BM) has a λ_{max} at 380 nm and a strong shoulder at 360 nm and two weaker peaks at 404 and 422 nm. Bowtie (BT) has a maximum absorption at 376 nm and low-energy resonances at 413 and 431 nm.[10] The two low-energy peaks in BM and BT appear to be similar to the two lowest energy absorption peaks of TR, while the stronger absorption peaks at higher energy are similar to the strong absorption peaks observed for the TR and the LC molecule. This suggests that the excitations in BM and BT have characteristics of both TR and LC. The red-shift in these peaks for BM and BT relative to those in TR and LC also suggest a strong intramolecular interaction in the macro-

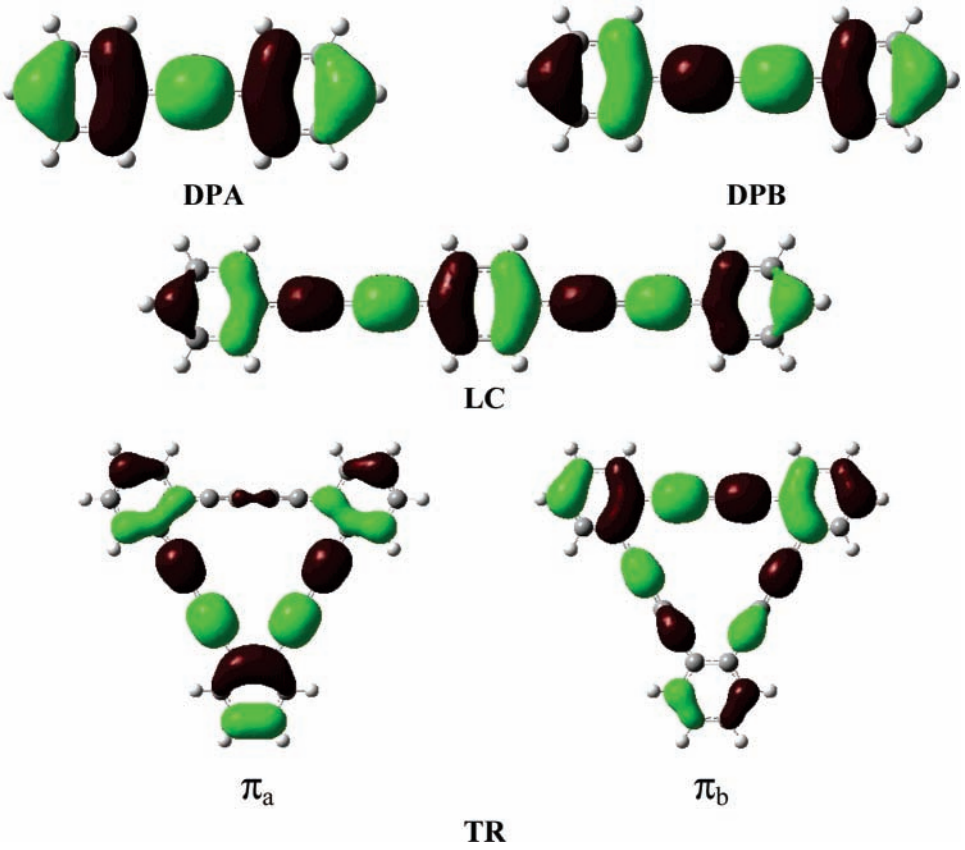

Figure 2. Highest occupied molecular orbital (HOMO) for DPA, DPB, LC, and TR at the B3LYP/6-31+G(d) level of theory (the HOMO in TR is a degenerate pair, orbitals π_a and π_b).

cycles. This qualitative, phenomenological analysis needs to be tested by quantum mechanical calculations as well as time-resolved (three-pulse photon echo) measurements as discussed below.

Energy Levels and Molecular Orbitals. To understand the excitation in the macrocycles better, it is necessary to first look at the molecular orbitals involved in the transition. The lowest electronic excitation in all these systems can be described primarily as a delocalized $\pi \rightarrow \pi^*$ transition. This involves the excitation of an electron from the HOMO to the LUMO. There is also a significant contribution from the $\pi' \rightarrow \pi'^*$ excitation (involving the π orbitals of the triple bonds lying in the σ plane of the rings and localized on the polyyne fragment), which is of the same symmetry as the $\pi \rightarrow \pi^*$ transition. Figure 2 shows the HOMO for the DPA, DPB, LC, and TR systems. The shapes of the frontier orbitals are nearly identical at the HF and B3LYP levels of theory. The π orbitals are delocalized, and the conjugation between the triple bonds and the aromatic rings can be seen clearly.

Inspection of the changes in the orbitals on going from DPA to DPB shows that each orbital splits into two—a symmetric and an anti-symmetric—combinations. This is seen better in Figure 3a, which shows the relevant orbital energy levels of DPA, DPB, LC, and TR. The calculations show that the size of the HOMO−LUMO gaps and the splitting between individual levels depends on the theory and basis set, but the overall pattern remains the same. Due to the splitting of the orbitals, the HOMO−LUMO gap decreases on going from DPA to DPB to LC, and thus the excitation energy decreases. The magnitude of the splitting and the shift in the lowest energy absorption peak are measures of the conjugation in these systems.

One of the key questions to be addressed is whether the excitations in the larger systems such as TR, BM, and BT are localized on a DPB fragment or delocalized over larger subunits or delocalized over the whole molecule. Figure 2 shows clearly

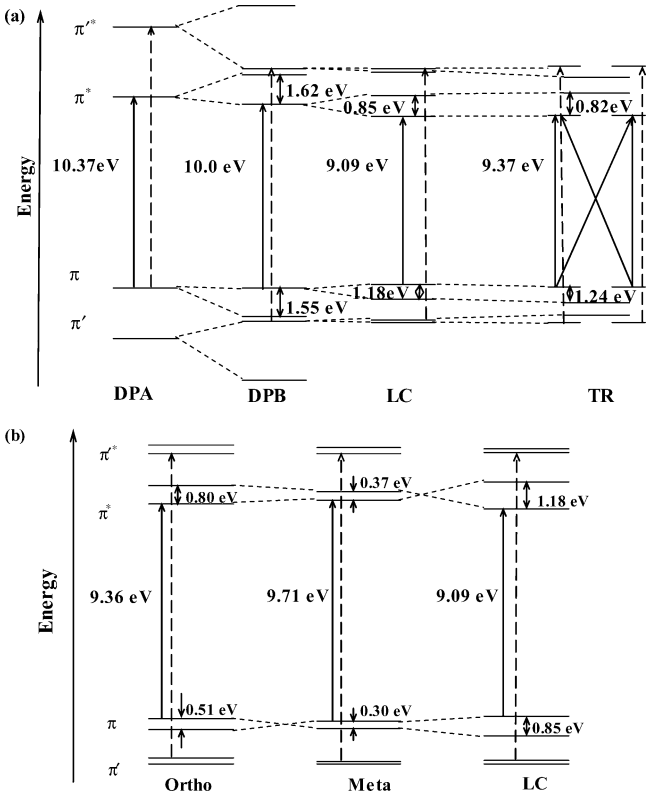

Figure 3. Orbital energy level diagrams for (a) DPA, DPB, LC, and TR. (b) O, M, and LC (the HOMO−LUMO gap and the splitting between the orbitals in eV is shown).

TABLE 2: Calculated Vertical Excitation Energies for the Lowest Transitions[a]

	CIS/3-21G	CIS(D)/3-21G	TD-B3LYP/STO-3G	TD-B3LYP/3-21+G	TD-B3LYP/6-31+G(d)	exp[b]
DPA	5.39 (230)	5.93(209)	4.97 (249)	4.22 (293)	4.07 (303)	4.14 (299)
DPB	4.87 (254)	5.64(219)	4.41 (281)	3.70 (334)	3.57 (347)	3.75 (330)
LC	4.51 (275)	5.12(242)	3.74 (330)	3.09 (400)	2.98 (415)	3.44 (360)
TR1[c]	4.44 (280)	5.06 (245)	3.67 (337)	3.07 (404)	2.94 (421)	3.35 (370)
TR2[c]	5.87 (212)	4.84 (257)	3.73 (332)	3.13 (396)	3.04 (407)	3.44 (360)
TR3	4.89 (253)	5.58 (222)	4.03 (307)	3.42 (362)	3.29 (376)	3.73 (332)
BM1			3.23 (383)	2.65 (468)		2.94 (422)
BM2			3.24 (382)	2.68 (462)		3.07 (404)
BM3			3.48 (356)	2.92 (424)		3.39 (366)
BT1			3.15 (393)	2.58 (481)		2.88 (431)
BT2			3.19 (388)	2.64 (469)		3.00 (413)
BT3			3.51 (353)	2.92 (242)		3.29 (376)

[a] Excitation energies in eV; values in parentheses correspond to wavelength in nm. [b] From the absorption spectrum shown in Figure 1. [c] The 0−1 transition (see Table 3 for details).

that the frontier orbitals are not localized on individual arms. The HOMO and LUMO for the triangular system are degenerate pairs of π orbitals designated π_a, π_b, and π_a^*, π_b^*, respectively. The orbitals in the triangle are fully delocalized, and the splitting between the HOMO and HOMO-1 and between the LUMO and LUMO+1 are nearly the same as in the LC molecule. In LC, the two DPB units are joined together in a para orientation. When the two DPB units are connected in the ortho and meta orientations, the splitting is smaller. In particular, the splitting in the ortho system is about two-thirds of that in the LC system. Thus the conjugation in O and M is not as strong as in LC, and the decrease in the HOMO−LUMO gap in these systems (compared to DPB) is not as large as in LC (Figure 3b). The TR can be considered as three DPB units joined together at the ortho position of the phenyl rings. Although the conjugation is not as strong for the ortho linkage, there are three nearest-neighbor interactions. When combined, these three interactions yield an orbital splitting for TR similar to the LC molecule, indicating that the strength of the conjugations in these molecules is comparable. This issue of delocalization in para versus meta conjugation has also been investigated in organic dendritic structures and studied in phenylacetylene dendrimers by Kopelman et al.[45] Melinger et al.[46] have likewise addressed the issue of conjugative interactions in ortho-, meta-, and para-substituted phenyl acetylene and dendrimers constructed from these systems. Martinez and co-workers[47] have studied the meta conjugation and coupling in the excited states in phenyl acetylene dendrimers.

Theoretical Investigation of the Absorption Spectra. The 0−0 transition energies for the lowest $\pi \rightarrow \pi^*$ transitions calculated by the CIS, CIS(D), and TD-B3LYP methods are collected in Table 2. The CIS method for excited states can be compared to Hartree−Fock theory for the ground state. Overall trends should be reproduced well, but details require a more sophisticated treatment. The CIS(D) method provides a second-order perturbation correction to the CIS excitation energies. More accurate methods such as CASSCF,[48−50] CASPT2,[51−53] and EOM-CCSD[54] would be desirable, but these are too expensive for the large molecules considered in the present work. An alternative is the time-dependent density functional theory (TD-DFT). The TD-DFT method performs well for valence excited states and can be applied to quite large systems. However, there are systematic errors with the extended conjugation and charge-transfer states, and these errors grow with the size of the system.[55−57]

As seen in Table 2, the calculated values of the individual excitation energies depend strongly on the method and the basis set. However, the overall trends in the calculations are in good agreement with the experimental energies, showing progressively lower excitation energies as the size of the molecules increases. Figure 4 shows a plot of the excitation energies calculated by the CIS(D)/3-21G, TD-B3LYP/3-21+G, and TD-B3LYP/6-31+G(d) methods versus the experimental excitation energies. There is a good correlation between the calculated and experimental excitation energies, indicating that the various levels of theory reproduce the key features of the absorption spectrum.

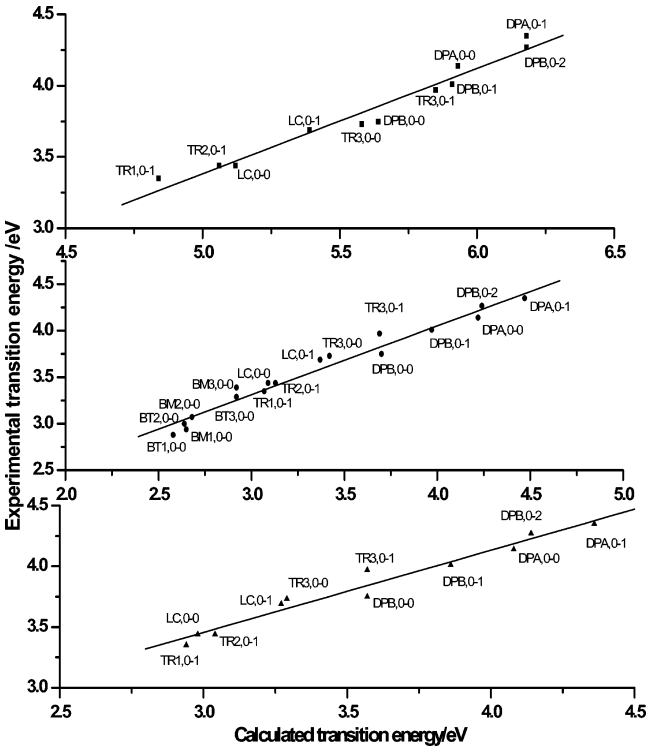

Figure 4. Comparison of calculated vs experimental transition energies (see Tables 2 and 3 for notation).

Localized versus Delocalized. The question of localized versus delocalized transitions in the absorption spectra can be addressed by examining the total electron density difference between the ground state and the excited state. Figure 5 shows the density difference plots for the lowest excited states of DPA, DPB, LC, and TR computed at CIS/3-21G. Since the HOMO and LUMO in TR are degenerate orbitals (E″ symmetry), single excitations from HOMO to LUMO give rise to four transitions of A'_1, A'_2, and E′ symmetry. For the degenerate E′ transition, the two density difference plots have been summed. The delocalized nature of the excitations in each of the four molecules can be clearly seen from this figure. When TR is distorted along selected vibrational modes, the density difference

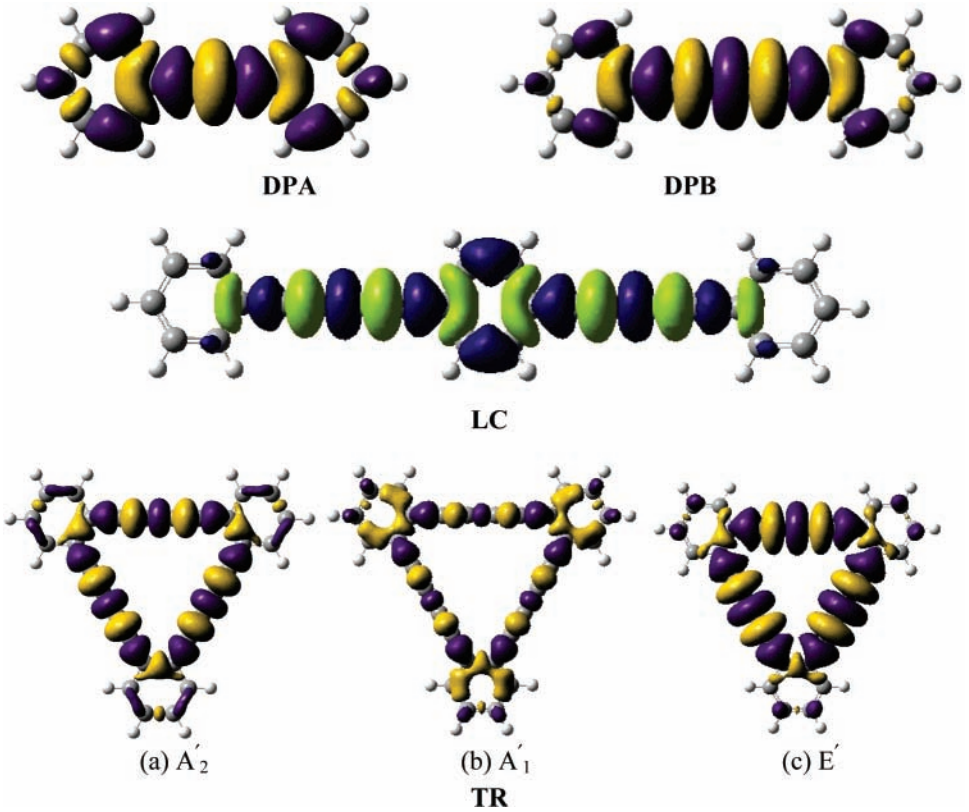

Figure 5. Density difference between the first excited state at CIS/3-21G and the ground HF/3-21G state for DPA, DPB, LC, and TR. The darker (purple) color shows increased electron density in the excited state and the lighter (green) color shows decreased electron density relative to the ground state.

plots remain fully delocalized. Even though the most intense peaks of DPB and TR coincide, the present electronic structure calculations indicate that lowest vertical excitations for TR are not localized to individual DPB units but are fully delocalized over the entire molecule.

Excitation Energies. Details of the calculated and experimental excitation energies and oscillator strengths are collected in Table 3. For benzene, the excitation energy of the E_{1u} state calculated at the TD-B3LY/6-31+G(d) level of theory are within 0.02 eV of the experimental values, and the calculated oscillator strengths are within about 30% of the experimental value.[58] The CIS method overestimates the excitation energy by nearly 2 eV and the oscillator strength by about 20%. On going from DPA to DPB, the first $^1A_g \rightarrow {}^1B_u$ band is red-shifted (0.4 eV experimentally, 0.3−0.5 eV calculated) as expected due to the decrease in HOMO−LUMO gap resulting from increased conjugation. In addition to the $\pi \rightarrow \pi^*$ transition, DPB has an intense $\pi' \rightarrow \pi'^*$ transition. The present calculations are consistent with the results of Hoshi et al.[20] at the PPP level of theory. However, the PPP calculations are unable to account for the mixing of the $\pi \rightarrow \pi^*$ and $\pi' \rightarrow \pi'^*$ transitions. Since the LC has more extended conjugation, the 0−0 transition shows a larger red-shift relative to DPA (0.7 eV experimentally, 0.8−1.1 eV calculated). In the triangular molecule, the only transition calculated to have a large oscillator strength in this region has $^1A'_1 \rightarrow {}^1E'$ symmetry. In the CIS(D) calculations, this transition comes at the same energy as obtained for DPB, just as is seen experimentally. The TD-B3LYP calculations of this transition are red-shifted as compared to DPB. This is a manifestation of the systematic error seen in the polyenes in which the lowest transitions show a greater red-shift as the length of the molecules is increased.[55] In the CIS(D)/3-21G and TD-B3LYP calculations, there are also two additional low-energy transitions $^1A'_1 \rightarrow {}^1A'_1$ and $^1A'_1 \rightarrow {}^1A'_2$. The CIS method places the $^1A'_1$ excited state at higher energy than the $^1E'$, but the more accurate methods, CIS(D) and TD-B3LYP, put both the $^1A'_1$ and $^1A'_2$ excited states at lower energy than the $^1E'$ state. More accurate calculations would be needed to determine whether the $^1A'_2$ state is lower in energy than the $^1A'_1$ state and to calculate the spacing between these states. Both the $^1A'_1 \rightarrow {}^1A'_1$ and $^1A'_1 \rightarrow {}^1A'_2$ transitions have zero electric dipole oscillator strength by symmetry. These will be discussed in more detail below. In the BM and BT molecules (see Table 2), the most intense 0−0 transition is red-shifted when compared to the intense transition in the triangle (ca. 0.4 eV experimentally, 0.5 eV calculated) indicating more extensive conjugation. In addition, there are two peaks at a lower energy that have significant oscillator strength. The ratio of the calculated oscillator strengths of the two low-energy peaks to that of the most intense peak is ∼0.1−0.2 as compared to an observed ratio of 0.4 in the extinction coefficients.

Vibrational Progression. The excitations in all the molecules studied here are accompanied by the lengthening of the C≡C bond (see Table 1). Because the lengthening of the C≡C bond in DPA and DPB are comparable, both show a similar vibrational progression. There is also a prominent vibrational progression clearly visible in LC. Comparison with DPA and DPB suggests that the second intense peak in the experimental spectrum of TR is also the result of a vibrational progression. The spacing in TR (1930 cm^{-1}) is comparable to that observed in DPA, DPB, and LC (2150 cm^{-1}) and is consistent with a vibrational progression in the symmetric C≡C stretch. The excited states for DPA, DPB, LC, and TR were optimized at the TD-B3LYP level of theory with the STO-3G and 3-21+G basis sets (Table 1). The differences in the ground- and excited-state geometries were decomposed in terms of the ground-state normal modes of vibration (similar results were obtained using

TABLE 3: Energies, Oscillator Strengths, and Description of the Calculated Transitions in DPA, DPB, LC, and TR

description[a]		transition energy (eV) CIS(D)/ 3-21G	TD-B3LYP/ 3-21+G	TD-B3LYP/ 6-31+G(d)	exp	oscillator strength[a] CIS(D)/ 3-21G	TD-B3LYP/ 3-21+G	TD-B3LYP/ 631+G(d)
				Diphenyl Acetylene (DPA)				
$^1A_g \rightarrow {}^1B_{1u}$	0−0	5.93	4.22	4.08	4.14	0.61	0.67	0.65
$\pi \rightarrow \pi^* + \pi' \rightarrow \pi'^*$	0−1[b]	6.18	4.47	4.33	4.35	0.23	0.25	0.24
	0−2[b]	6.43	4.72	4.58		0.04	0.05	0.04
				Diphenyl Butadiyne (DPB)				
$^1A_g \rightarrow {}^1B_{1u}$	0−0	5.64	3.70	3.57	3.75	0.35	0.52	0.49
$\pi \rightarrow \pi^* + \pi' \rightarrow \pi'^*$	0−1[c]	5.91	3.97	3.84	4.01	0.23	0.34	0.33
	0−2[c]	6.18	4.24	4.11	4.27	0.07	0.11	0.10
$^1A_g \rightarrow {}^1B_{1u}$	0−0	−	5.71	5.53	4.77	−	1.09	1.14
$\pi' \rightarrow \pi'^* - \pi \rightarrow \pi^*$								
				Long Chain (LC)				
$^1A_g \rightarrow {}^1B_{1u}$	0−0	5.12	3.10	2.98	3.44	1.28	1.58	1.53
$\pi \rightarrow \pi^* + \pi' \rightarrow \pi'^*$	0−1[c]	5.39	3.37	3.25	3.69	0.52	0.64	0.62
	0−2[c]	5.66	3.64	3.52	−	0.11	0.13	0.13
$^1A_g \rightarrow {}^1B_{1u}$	0−0	−	5.64	5.44	4.59		2.43	2.46
$\pi' \rightarrow \pi'^* - \pi \rightarrow \pi^*$								
				Triangle (TR)				
$^1A'_1 \rightarrow {}^1A'_2$(TR1)	0−0	4.93	2.94	2.81	−	0.00	0.00	0.00
$\pi_a \rightarrow \pi_b^* + \pi_b \rightarrow \pi_a^*$	0−1[d]	5.06	3.07	2.94	3.35	2×10^{-3}	0.0022	−
$^1A'_1 \rightarrow {}^1A'_1$(TR2)	0−0	4.76	3.05	2.95	−	0.00	0.00	0.00
$\pi_b \rightarrow \pi_b^* - \pi_a \rightarrow \pi_a^*$	0−1[e]	4.84	3.13	3.04	3.44	1×10^{-3}	0.0022	−
$^1A'_1 \rightarrow {}^1E'$ (TR3)	0−0	5.58	3.42	3.29	3.73	1.32	1.12	1.14
$\pi_a \rightarrow \pi_b^* - \pi_b \rightarrow \pi_a^*$	0−1[f]	5.85	3.69	3.56	3.97	0.38	0.32	0.33
$\pi_a \rightarrow \pi_a^* + \pi_b \rightarrow \pi_b^*$ [g]								

[a] For vibrational progressions, the oscillator strengths are multiplied by the Franck−Condon factors (see Table 4). [b] Assuming a progression in the C≡C stretch (using a spacing of 2049.6 cm^{-1} obtained from CIS/3-21G calculation on the excited state of DPA). [c] Assuming a progression in the C≡C stretch (using a spacing of 2164.8 cm^{-1} obtained from CIS/3-21G calculation on the excited state of DPB). [d] Vibronic coupling involving a e′ vibration (estimated using the ground-state vibrational mode at 1090.1 cm^{-1} at HF/3-21G and 1027.12 cm^{-1} at B3LYP/3-21G). [e] Vibronic coupling involving a e′ vibration (estimated using the ground-state vibrational mode at 690.76 cm^{-1} at B3LYP/3-21G). [f] Assuming a progression in the C≡C stretch (using a spacing of 2164.8 cm^{-1} obtained from CIS/3-21G calculation on the excited state of DPB). [g] The second member of the degenerate pair.

TABLE 4: Ground-State Vibrational Frequencies and Franck−Condon (FC) Factors

molecule	frequency (unscaled)	FC factor (eq 2) $\upsilon = 0$	$\upsilon = 1$	$\upsilon = 2$
DPA[a]	1052.9	0.845	0.142	0.012
	1212.3	0.752	0.214	0.030
	1732.3	0.718	0.237	0.039
	2467.4	0.589	0.311	0.082
DPA[b]	1022.9	0.826	0.157	0.014
	1166.6	0.837	0.149	0.013
	1615.9	0.771	0.200	0.026
	2315.9	0.688	0.257	0.048
DPB[a]	1052.1	0.938	0.059	0.001
	1732.6	0.913	0.083	0.003
	2453.8	0.187	0.314	0.263
DPB[b]	990.6	0.884	0.109	0.006
	1617.8	0.871	0.119	0.008
	2339.2	0.519	0.340	0.111
LC[a]	1026.7	0.857	0.132	0.010
	1722.1	0.788	0.187	0.022
	2443.5	0.665	0.271	0.055
TR[a]	1011.8	0.883	0.109	0.006
	1582.3	0.913	0.082	0.003
	2384.4	0.748	0.217	0.031

[a] TD-B3LYP/STO-3G data. [b] TD-B3LYP/3-21+G data.

the excited-state normal modes). The Franck−Condon factors were calculated using eq 2, and values for the more prominent vibrational progressions are listed in Table 4. As seen from the table, the symmetric C≡C stretching frequency (∼2400 cm^{-1}) is the most active FC mode. For BM and BT, the most intense peaks are red-shifted as compared to TR and would also appear to show one or more vibrational progressions. However, the overlap in this part of the spectra makes it more difficult to discuss these in detail.

Photon Echo Experiments. The observed oscillator strengths of the two low energy peaks in the absorption spectrum of the BM molecule were approximately two times greater than that found for the TR system's lower energy peaks. This intriguing finding, was further investigated by three-pulse photon echo measurements. Measurements were carried out in vicinity (417 nm) of the two low-energy peaks observed in the absorption spectrum of BM.

Shown in Figure 6 are the three-pulse-photon echo scans of the BM system at population times ∼0 fs and 33 ps for the two different phase matching directions. It was noted that the echo intensity (at a particularly low optical density at 417 nm) was very high. The intensity was significantly larger than what was obtained with β-carotene with the same optical density. This may be an indication of the relative magnitudes of the transition dipole moment as well as the dephasing time for the BM molecule.[59] The transition moment for the BM may be a result of the delocalized state involving the chromophore building blocks constituting two triangular molecules (or a molecule longer than the LC) and subsequently a larger echo intensity is anticipated. The decay of the echo intensity may also give information regarding the characteristics of the delocalized states in BM as well. At population time 33 ps the echo was fit to a Gaussian with a fwhm of ∼70 fs. Previous reference measurements with β-carotene (which has been reported to have a dephasing time of 4 fs)[60] gave an echo fwhm of ∼65 fs. The

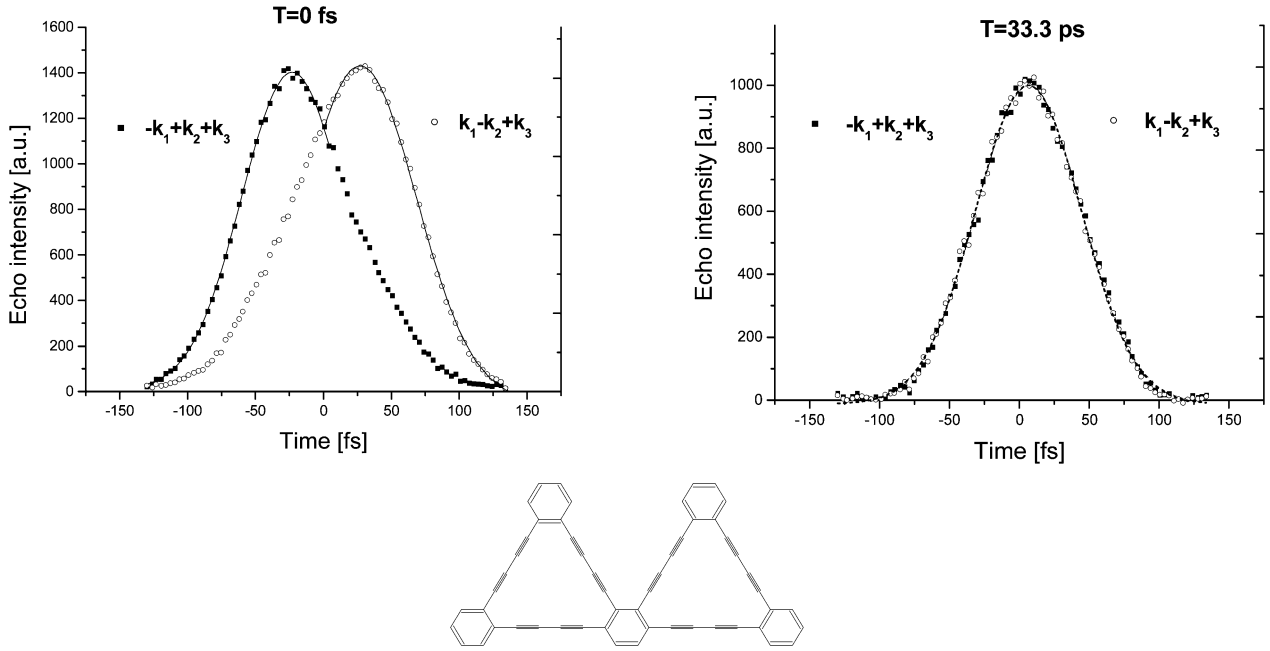

Figure 6. 3-pulse photon echo for the BM.

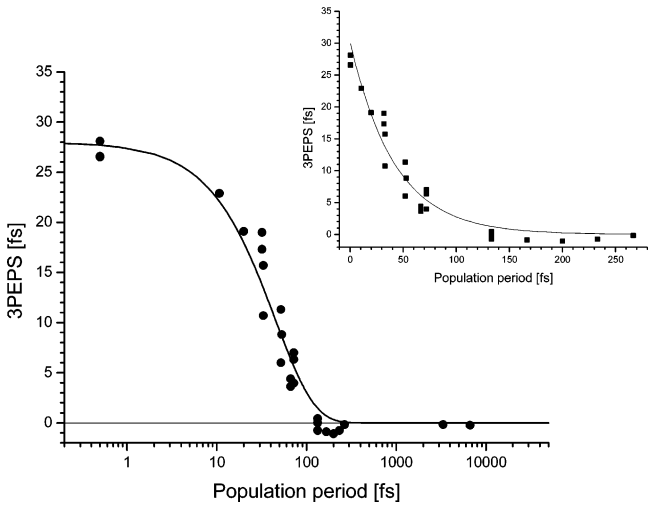

Figure 7. 3-pulse photon echo peak shift.

dephasing time of the BM can be estimated to be ~50 fs within the time resolution of our experiment and analysis. However, at room temperature strong electron−phonon coupling and complex non-Markovian dynamics of the system make the description of the electronic dephasing more complicated.[61] A more detailed measure of the system dynamics may be obtained from the three-pulse photon echo peak shift method (3PEPS).[28,29,32,33]

Shown in Figure 7 is the 3PEPS result as a function of population time *T*. As it can be observed from the figure, there is a relatively large initial peak shift value at $T = 0$, which drops to zero as *T* rises above 100 fs. An initial peak shift value of ~28 fs was obtained for the BM system at room temperature measured at 417 nm. The BM system's initial peak shift is comparable to that reported for BIC J-aggregates (28 fs)[62] as well as for PIC J-aggregates.[63] The initial peak shift value observed for BM at room temperature compares with other well-investigated systems, which demonstrated relatively weak coupling to the bath.[30,62,63] The presence of a large peak shift is an indication of a relatively weak electron phonon (vibronic) coupling in this carbon-rich system. It is established that the 3PEPS as a function of population time *T* closely follows the shape of a transition frequency correlation function.[28,29] Fast decaying correlation function approaches the δ-shaped correlation function of the Bloch model (fast modulation limit). However, numerical simulation of our photon echo peak shift data using Brownian oscillator model[59] showed that the system remains in slow modulation limit, when the time scale of nuclear motions $1/\Lambda$ is slower than compared with the magnitude of transition frequency fluctuations (coupling strength Δ). The ratio $k = \Lambda/\Delta$ was estimated to be $\sim 0.4 < 1$ in our case. This result is in agreement with the observed Gaussian shape of both absorption lines of the doublet, while the static inhomogeneous broadening is negligibly small (see below). The initial fast decay of the photon echo peak shift (~27 fs) for the BM molecule is also comparable to that observed for BIC J-aggregates, where the decay was found to have time constants of 26 and 128 fs.[62] It was suggested that the fast decay of 26 fs might be due to inertial component in the water. Joo et al.[63] observed single-exponential decay of photon echo peak shift of PIC J-aggregates with a time constant of ~107 fs and suggested that origin of this decay is due to mechanisms involving exciton−phonon scattering processes. Another interesting feature of the peak shift decay for the BM is the absence of intermediate time scale decay components and a very small 3PEPS value right after 200 fs. It was shown[29,33] that the nonzero residual value of the peak shift indicates the presence of static disorder (inhomogeneous broadening) in the system. For the BM annulene the peak shift decayed to zero, suggesting that there is little or no contribution to inhomogeneous broadening; thus, the system is effectively homogeneous after ~100 fs at room temperature in solution. This may be due to the rigid homogeneous structure as well as due to the possibility of a motional narrowing effect as was observed in the exciton description of J-aggregates.[62,63]

Interpretation of the Calculated Absorption Spectra

In the BM and the BT, the two transitions at lower energy are allowed by symmetry and have nonzero intensities. This is supported by the large photon echo signal observed for the BM. At the TD-B3LYP/3-21+G level of theory, the oscillator strengths for these transitions are 10−20% of the most intense transition. Experimentally, the extinction coefficients for the low-energy peaks are about 40% of the most intense peak. To

obtain better agreement with the experimental intensities for BM and BT, calculations with larger basis sets would be needed, but these are not practical at this time. The experimental spectrum of the TR molecule (Figure 1) also shows two smaller peaks at energies lower than the most prominent band and with intensities 30% of the most intense peak. The CIS(D) and TD-B3LYP calculations indicate two $\pi \rightarrow \pi^*$ transitions in this region, but they have zero oscillator strength due to symmetry. As an attempt to understand how the two peaks of TR gain intensity, we looked at two possible mechanisms: thermal excitation and vibronic coupling. For the bis-annulenes, we would like to understand the spectra of BM and BT in terms of the TR and DPB subunits. Therefore, we developed a simple exciton model to examine the interaction of the DPB units that form the TR and the TR units that form the BM and BT systems.

Origin of the Two Low-Energy Peaks in the Spectrum of TR. The HOMO and LUMO of TR are both doubly degenerate orbitals with E″ symmetry, hence four states can be generated from a HOMO → LUMO excitation. A similar situation arises in benzene.[44] The symmetries of these four states are $E'' \times E'' = A'_1 + A'_2 + E'$. The transition to the E′ state is dipole allowed as mentioned above and accounts for the most intemse peak in the spectrum. The transitions from the ground state to the A'_1 and A'_2 states are dipole forbidden and hence have zero oscillator strength. The spacing between the two low intensity peaks is 750 cm^{-1}. This is much smaller that the spacing seen in the vibrational progression in the E′ state. The data from Table 4 also do not reveal any significant vibrational progression involving frequencies in this range. Thus it is unlikely that these two peaks arise from an excitation to a single state with a vibrational progression. Furthermore, a vibrational progression due to Franck−Condon overlap cannot lead to any intensity for these transitions.

As indicated above, the triangle molecule is flexible, and it is possible that thermal excitation of ground-state vibrations may contribute to the intensity of the low-energy peaks. For thermal displacements in the harmonic approximation, the effective oscillator strengths can be calculated using eqs 7 and 8. By symmetry, only the transition dipole derivatives with respect to the e′ vibrational modes are nonzero and contribute to $\partial^2 f/\partial x_i^2$. The derivatives of the transition dipole moments were calculated numerically at the TD-B3LYP/STO-3G level of theory. The molecule was displaced along each of the e′ normal modes, and the transition dipole was recalculated. The data are collected in Table 5 and show that the contributions to the intensity from zero point vibration and thermal excitation are small in the harmonic oscillator approximation. This approach is probably appropriate only for the low-frequency modes. Even though the mean squared displacement can be sizable for the low-frequency modes, the transition dipole derivatives are small. However, each of the low-frequency modes can contribute and the sum of the values is significant. Molecular dynamics simulations would permit better estimations of the intensities beyond the approximation of the harmonic vibrations and linear dependence of the transition dipole. If this is the mechanism by which these peaks gain intensity, then changes in temperature and solvent viscosity should alter the intensity of the peaks in the experimental spectrum.

Another mechanism by which dipole forbidden bands can gain intensity is through vibronic coupling. The situation in TR is analogous to benzene, where the doubly degenerate HOMO and LUMO orbitals give rise to B_{2u}, B_{1u}, and E_{1u} symmetry excited states. Transitions from the ground state to the B_{2u} and B_{1u} states are dipole forbidden but gain intensity due to vibronic coupling with e_{2g} symmetry vibrational modes.[44] In TR, the corresponding transitions have $^1A'_1 \rightarrow {}^1A'_2$ and $^1A'_1 \rightarrow {}^1A'_1$ symmetry and can couple to normal modes of e′ symmetry to gain intensity. The STO-3G data in Table 5 serves as a guide. The molecule was displaced along several e′ modes (frequencies of 744, 826, 1091, and 2466 cm^{-1} for CIS(D)/3-21G and 691, 775, 1027, 2257, and 2351 cm^{-1} for TD-B3LYP/3-21+G). These modes are the distortion of the benzene rings and the C≡C stretching. The $^1A'_1 \rightarrow {}^1A'_2$ transition gains intensity primarily due to coupling with the C≡C stretching and also by coupling to ring distortion modes. The $^1A'_1 \rightarrow {}^1A'_1$ transition couples to the ring distortion mode at 691 cm^{-1}. However, the vibronic coupling calculations yield relative intensities that are 2 orders of magnitude smaller than seen in the experimental spectrum. Thus the two smaller peaks observed at lower energies in the experimental spectrum of the TR could be attributed to either vibronic coupling in the excited state or thermal motion in the ground state. However, neither mechanism predicts intensities comparable to experiment.

TABLE 5: Vibrational Frequencies,[a] Transition Dipole Derivatives, and Thermal and Vibronic and Contribution to the Intensity for the A'_2 and A'_1 Excited States of TR

frequency (in cm^{-1})	$(2m\omega_{ge}(\partial\mu_{ge}/\partial x)^2)/3e^2\hbar$ (in $Å^{-2}$)	thermal averaged (eq 8)	vibronic coupling (eq 5)
	A'_2 State		
180.2	0.037	1.28×10^{-3}	5.27×10^{-4}
521.7	0.050	2.19×10^{-4}	1.87×10^{-4}
582.3	0.097	3.19×10^{-4}	2.83×10^{-4}
692.3	0.007	2.91×10^{-5}	2.71×10^{-5}
786.4	0.175	6.15×10^{-4}	5.88×10^{-4}
1031.4	0.800	1.63×10^{-3}	1.60×10^{-4}
1274.4	0.970	5.07×10^{-3}	5.05×10^{-3}
1421.8	0.107	3.93×10^{-4}	3.93×10^{-4}
1557.7	0.100	4.52×10^{-4}	4.51×10^{-4}
1582.1	2.850	1.01×10^{-2}	1.01×10^{-2}
1675.1	2.175	4.43×10^{-3}	4.43×10^{-3}
1716.3	4.125	7.52×10^{-3}	7.51×10^{-3}
2384.0	4.552	2.68×10^{-3}	2.68×10^{-3}
	A'_1 State		
180.2	0.007	2.57×10^{-4}	1.05×10^{-4}
521.7	0.017	7.67×10^{-5}	6.53×10^{-5}
582.3	0.080	2.62×10^{-4}	2.32×10^{-4}
692.3	0.540	2.09×10^{-3}	1.95×10^{-3}
786.4	0.257	9.05×10^{-4}	8.65×10^{-4}
1031.4	0.295	5.99×10^{-4}	5.91×10^{-4}
1274.4	0.037	1.96×10^{-4}	1.95×10^{-4}
1421.8	0.027	1.00×10^{-4}	1.00×10^{-4}
1557.7	0.232	1.05×10^{-3}	1.04×10^{-3}
1582.1	0.127	4.54×10^{-4}	4.53×10^{-4}
1675.1	0.207	4.23×10^{-4}	4.23×10^{-4}
1716.3	0.847	1.54×10^{-3}	1.54×10^{-3}
2384.0	0.067	3.97×10^{-5}	3.97×10^{-5}

[a] Unscaled ground-state frequencies of e′ symmetry at B3LYP/STO-3G.

Exciton Model for the Annulenes and Bis-annulenes. To gain further insight into the excited states of the various conjugated systems, it is instructive to develop a simple exciton model. The various systems discussed above can be built from overlapping DPB units. The low lying excited states of these systems can be constructed from linear combination of excited configurations localized to individual DPB units and charge transfer (CT) excitations between neighboring DPB units. Because the DPB units are coupled, these excitations must be allowed to interact in a configuration interaction (CI) manner via an appropriate Hamiltonian. Harcourt et al.[64−66] have provided a detailed theoretical framework for constructing exciton models to describe excited-state interactions and energy

transfer processes. Alternatively, a very simple exciton model of larger molecules such as TR, BM, and BT can be constructed by obtaining the necessary matrix elements for the CI Hamiltonian by fitting to the excited-state calculations of smaller molecules that contain DPB units in the appropriate orientations.

In a simple model, the lowest excited states of a DPB unit can be constructed from its highest occupied π orbital and lowest unoccupied π^* orbital. These orbitals can be used to describe the excitations of the DPB units in the O, M, LC, and TR molecules. The TD-DFT calculations conform best to this simple model. Hence, the eigenvalues and approximate eigenvectors from these calculations were used to build an approximate Hamiltonian in the π MO basis. The MO values were assumed to be simple symmetry adapted combinations of localized π and π^* orbitals (e.g., for LC, $\pi_1 \pm \pi_2$ and $\pi_1^* \pm \pi_2^*$).

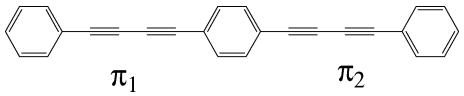

The Hamiltonian was transformed into the localized basis of excitations on a single DPB unit, $\pi_1 \rightarrow \pi_1^*$, $\pi_2 \rightarrow \pi_2^*$, and charge-transfer excitations between neighboring DPB units, $\pi_1 \rightarrow \pi_2^*$, $\pi_2 \rightarrow \pi_1^*$.

In the first stage of the analysis, the various TD-DFT calculations on O, M, and LC were used to construct a simple exciton model for comparison with the calculations on TR, BM, and BT. The matrix elements from the ortho system are sufficient to describe the interactions between two of the DPB units in TR. However, to complete the exciton model for the TR molecule, some additional matrix elements are needed that cannot be obtained from the ortho system. These are coupling matrix elements between CT excitations that involve all three DPB units in the TR molecule. Specifically, the elements are of the type H($\pi_1 \rightarrow \pi_2^*$, $\pi_2 \rightarrow \pi_3^*$), H($\pi_1 \rightarrow \pi_2^*$, $\pi_3 \rightarrow \pi_2^*$) and H($\pi_1 \rightarrow \pi_2^*$, $\pi_1 \rightarrow \pi_3^*$).

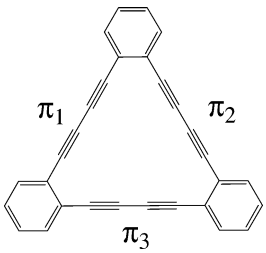

These matrix elements were assigned the same magnitude and this magnitude was adjusted to obtain a similar splitting between the two lowest states of TR as in the TD-DFT calculations. Without these matrix elements, the A'_2 state is predicted to be higher in energy than the E′ state.

The simple exciton model is in very good agreement with the TD-DFT calculations for O, M, and LC because they were used to derive the matrix elements. For TR, the energies are within 0.15 eV of the corresponding TD-DFT calculations, except for the highest state. When this model is applied to the BM and BT systems, it predicts the first excited state to be ca. 0.6 eV lower than in LC. This compares quite favorably to the experimentally observed lowering of 0.50−0.56 eV. The next 10 states are within 0.2 eV of the TD-DFT values, showing that the exciton model captures the important trends in these systems.

In a second stage, a better exciton model was obtained by fitting to calculations on O, M, LC, and TR. This exciton model yields energies within 0.07 eV of the corresponding TD-DFT calculations for all of the π excitations considered in O, M, LC, and TR. When compared to TD-DFT/3-21+G calculations on BM and BT, the mean absolute deviation for the first 15 states of each molecule is 0.11 eV. The various matrix elements for this exciton model are summarized in Table 6. The diagonal elements for the $\pi \rightarrow \pi^*$ excitations localized to a single DPB unit for the meta and para cases are chosen to be the same as determined for ortho. The magnitude of the CT energies are similar to the local $\pi \rightarrow \pi^*$ excitation; the CT energy for the ortho case is 0.29 eV smaller than for para. The interaction matrix elements between the various localized excitations range from −0.45 eV to +0.30 eV. The interactions are more stabilizing in the ortho and para geometries than in the meta orientation, reflecting the orbital interactions through the benzene ring that couples the two arms of the π systems in O, M, and LC.

TABLE 6: Matrix Elements for the Exciton Model Obtained by Fitting to the B3LYP/3-21+G TD-DFT Calculations (in eV)

type of matrix elements	ortho	meta	para
Diagonal Elements			
$\pi_1 \rightarrow \pi_1^*$ (localized on a single DPB unit)	3.754	3.754	3.754
$\pi_1 \rightarrow \pi_2^*$ (charge transfer between neighboring units)	3.695	3.739	3.989
Interaction Elements			
$\pi_1 \rightarrow \pi_1^*/\pi_2 \rightarrow \pi_2^*$	−0.099	−0.100	−0.017
$\pi_1 \rightarrow \pi_1^*/\pi_2 \rightarrow \pi_1^*$	0.307	0.103	−0.447
$\pi_1 \rightarrow \pi_1^*/\pi_1 \rightarrow \pi_2^*$	0.248	−0.075	−0.346
$\pi_1 \rightarrow \pi_2^*/\pi_2 \rightarrow \pi_1^*$	0.121	−0.105	0.044
$\pi_1 \rightarrow \pi_2^*/\pi_2 \rightarrow \pi_3^*$	−0.041	−0.041	−0.041
$\pi_1 \rightarrow \pi_2^*/\pi_3 \rightarrow \pi_2^*$	0.190	0.190	0.190
$\pi_1 \rightarrow \pi_2^*/\pi_1 \rightarrow \pi_3^*$	0.248	0.248	0.248
$\pi_1 \rightarrow \pi_1^*/\pi_2 \rightarrow \pi_3^*$	0.061	0.061	0.061

For the TR molecule, the lowest two states have A'_2 and A'_1 symmetry, respectively, and have zero oscillator strength in the CIS(D) and TD-DFT calculations. In the exciton model, the A'_2 state involves only CT excitations, $(\pi_1 \rightarrow \pi_2^* + \pi_2 \rightarrow \pi_3^* + \pi_3 \rightarrow \pi_1^*) - (\pi_1 \rightarrow \pi_3^* + \pi_3 \rightarrow \pi_2^* + \pi_2 \rightarrow \pi_1^*)$, and the electric dipole oscillator strengths of the individual excitations sum to zero by symmetry. The A'_1 state involves both localized $\pi \rightarrow \pi^*$ excitations as well as CT excitations, $(\pi_1 \rightarrow \pi_1^* + \pi_2 \rightarrow \pi_2^* + \pi_3 \rightarrow \pi_3^*) + \lambda(\pi_1 \rightarrow \pi_2^* + \pi_2 \rightarrow \pi_3^* + \pi_3 \rightarrow \pi_1^*) + \lambda(\pi_1 \rightarrow \pi_3^* + \pi_3 \rightarrow \pi_2^* + \pi_2 \rightarrow \pi_1^*)$, and oscillator strengths of these localized excitations also sum to zero by symmetry. As discussed above, the A'_2 and A'_1 states can gain some intensity through vibronic coupling and/or thermal vibrational motion. The lowest $\pi \rightarrow \pi^*$ transition with substantial intensity has E′ symmetry. In the exciton model this state involves a combination of localized $\pi \rightarrow \pi^*$ states and CT states.

Figure 8 shows the evolution of the states for TR, BM, and BT as the interactions are included in a stepwise fashion. When the interaction between a pair of neighboring DPB units is turned on, four states result. As expected, these are very strong interactions, accounting for about half of the spread in excitation energies seen in BM and BT. When a third DPB unit is brought in to complete the triangle, the interactions increase further and yield the nine states of TR. The lowest A'_1, A'_2, and E′ states of TR evolve from the lowest two states of the ortho molecule. By symmetry the E′ transition is dipole allowed but the A′ transitions are forbidden. Last, the two triangles are allowed to interact to form the BM and BT molecules. The lowest energy peaks arise from the two low-energy states in the triangle moieties interacting with each other. They gain intensity by also interacting with the E′ states of the triangles. The E′ states of the triangle moieties also interact strongly and account for the

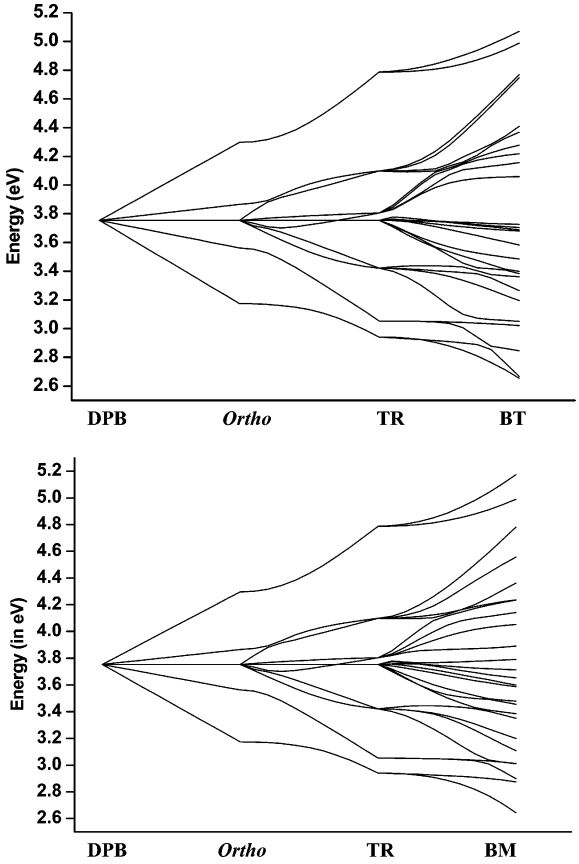

Figure 8. Evolution of the excitation energies from DPB to ortho to TR and to BM and BT as the appropriate interactions in the exciton model are turned on.

groups of intense peaks in the spectra. The eigenvectors from the exciton model indicate that the transitions in BM and BT are delocalized over the whole molecule and not localized on one of the TR units.

The simple exciton model is successful in capturing the main trends in these systems. There is a good correlation between the excitation energies predicted by the exciton model and the energies computed by TD-DFT calculations. This model can be used to study much larger systems built from DPB units. Thus, it is a useful and efficient tool to understand the excitations in such large conjugated systems.

Conclusion

From the comparison of the absorption spectra of molecules DPB, LC, TR, BM**,** and BT, we suggest that the excitations in BM and BT have the characteristics of TR and LC. The lowest energy absorption peaks in TR and BM may have contributions from vibronic and excitonic coupling. The present calculations show that the excitations in these systems are primarily delocalized $\pi \rightarrow \pi^*$ transitions involving electron transfer from the HOMO to the LUMO. From the shape of the molecular orbitals and electron density difference plots, it is clear that the transitions are delocalized over the whole system for all the molecules studied. The calculated excitation energies are in good qualitative agreement with the experimental values. On going from DPA to the larger molecules, the most intense 0−0 transition is red-shifted due to the increased conjugation. There is a strong vibrational progression in the transition and the symmetric C≡C stretching frequency is the most active FC mode. The results from the simple exciton model calculations are in good agreement with the TD-DFT calculations and reproduce the trends quite well. Our calculations (CIS(D), TD-DFT and exciton model) show that the two low-energy transitions in TR are not allowed by symmetry. However, these transitions may gain some intensity to vibronic coupling in the excited state or thermal motion in the ground state. The corresponding two transitions in BM and BT have nonzero intensities since they are allowed by symmetry and are computed to have significant intensity. The three-pulse photon echo measurements for BM further suggested a delocalized excitation with a relatively weak coupling to the bath (solvent interactions). The allowed transition in this system lead to a large photon echo intensity and a large initial three-pulse photon echo peak shift value. The small residual peak shift value (at longer population times) suggests that the contribution from real inhomogeneous broadening is small for BM. The measurements and calculations reported in the present study provide further insight into an interesting organic molecular architecture which may have optical and electronic applications in the future.

Acknowledgment. We thank the National Science Foundation (DMR-0134691 to T.G.III., CHE-0131157 to H.B.S., and CHE-0104854 to M.M.H.). T.G.III. and M.M.H. also thank The Camille and Henry Dreyfus Foundation (Teacher-Scholar Awards to M.M.H. (1998−2002) and T.G.III. (2002−2006)) for support of this research. J.A.M. acknowledges the Department of Education for a GAANN Graduate Fellowship. The authors are thankful to Sridhar Lahankar for assistance at the beginning of this investigation. The authors also thank NCSA and ISC (at WSU) for computer time.

Supporting Information Available: Experimental details for the synthesis of LC. This material available free of charge via the Internet at http://pubs.acs.org.

References and Notes

(1) Varnavski, O.; Goodson, T. *Chem. Phys. Lett.* **2000**, *320*, 688−696.

(2) Anderson, S.; Aplin, R. T.; Claridge, T. D. W.; Goodson, T.; Maciel, A. C.; Rumbles, G.; Ryan, J. F.; Anderson, H. L. *J. Chem. Soc., Perkins Trans. 1* **1998**, 2383−2397.

(3) Ispasoiu, R. G.; Balogh, L.; Varnavski, O. P.; Tomalia, D. A.; Goodson, T. *J. Am. Chem. Soc.* **2000**, *122*, 11005−11006.

(4) Pillow, J. N. G.; Burn, P. L.; Samuel, I. D. W.; Halim, M. *Synth. Met.* **1999**, *102*, 1468−1469.

(5) Hawker, C. J.; Frechet, J. M. J. In *New Methods of Polymer Synthesis*; Ebdon, J. R., Eastmond, G. C., Eds.; Blackie: Glasgow, UK, 1995; pp 290−330.

(6) Hawker, C. J.; Wooley, K. L. In *Advances in Dendritic Macromolecules*; Newkome, G. R., Ed.; Elsevier: New York, 1995; Vol. 2, pp 1−39.

(7) Varnavski, O. P.; Ostrowski, J. C.; Sukhomlinova, L.; Twieg, R. J.; Bazan, G. C.; Goodson, T. *J. Am. Chem. Soc.* **2002**, *124*, 1736−1743.

(8) Brunel, J.; Ledoux, I.; Zyss, J.; Blanchard-Desce, M. *Chem. Commun.* **2001**, 923−924.

(9) Haley, M. M.; Wan, W. B. In *Advances in Strained and Interesting Organic Molecules*; Halton, B., Ed.; JAI Press: New York, 2000; Vol. 8, pp 1−41.

(10) Wan, W. B.; Brand, S. C.; Pak, J. J.; Haley, M. M. *Chem. Eur. J.* **2000**, *6*, 2044−2052.

(11) Wan, W. B.; Haley, M. M. *J. Org. Chem.* **2001**, *66*, 3893−3901.

(12) Marsden, J. A.; Palmer, G. J.; Haley, M. M. *Eur. J. Org. Chem.* **2003**, 2355−2369.

(13) Haley, M. M.; Pak, J. J.; Brand, S. C. In *Topics in Current Chemistry*; de Meijere, A., Ed.; Springer-Verlag: Berlin, 1999; Vol. 201; pp 81−130.

(14) Baughman, R. H.; Eckhardt, H.; Kertesz, M. *J. Chem. Phys.* **1987**, *87*, 6687−6699.

(15) Narita, N.; Nagai, S.; Suzuki, S.; Nakao, K. *Phys. Rev. B* **1998**, *58*, 11009−11014.

(16) Narita, N.; Nagai, S.; Suzuki, S.; Nakao, K. *Phys. Rev. B* **2000**, *62*, 11146−11151.

(17) Narita, N.; Nagai, S.; Suzuki, S. *Phys. Rev. B* **2001**, *64*, 245408.

(18) Birckner, E.; Grummt, U. W.; Goeller, A. H.; Pautzsch, T.; Egbe, D. A. M.; Al-Higari, M.; Klemm, E. *J. Phys. Chem. A* **2001**, *105*, 10307−10315.
(19) Sarkar, A.; Pak, J. J.; Rayfield, G. W.; Haley, M. M. *J. Mater. Chem.* **2001**, *11*, 2943−2945.
(20) Hoshi, T.; Okubo, J.; Kobayashi, M.; Tanizaki, Y. *J. Am. Chem. Soc.* **1986**, *108*, 3867−3872.
(21) Hirata, Y.; Okada, T.; Nomoto, T. *Chem. Phys. Lett.* **1998**, *293*, 371−377.
(22) Hirata, Y.; Okada, T.; N., M.; Nomoto, T. *J. Phys. Chem.* **1992**, *96*, 6559−6563.
(23) Ferrante, C.; Kensy, U.; Dick, B. *J. Phys. Chem.* **1993**, *97*, 13457−13463.
(24) Karabunarliev, S.; Baumgarten, M.; Muellen, K. *J. Phys. Chem. A* **2000**, *104*, 8236−8243.
(25) Beeby, A.; Findlay, K.; Low, P. J.; Marder, T. B. *J. Am. Chem. Soc.* **2002**, *124*, 8280−8284.
(26) Sluch, M. I.; Godt, A.; Bunz, U. H. F.; Berg, M. A. *J. Am. Chem. Soc.* **2001**, *127*, 6447−6448.
(27) Levitus, M.; Schmieder, K.; Ricks, H.; Shimizu, K. D.; Bunz, U. H. F.; Garcia-Garibay, M. A. *J. Am. Chem. Soc.* **2001**, *123*, 4259−4265.
(28) de Boeij, W. P.; Pshenichnikov, M. P.; Wiersma, D. A. *Chem. Phys. Lett.* **1996**, *253*, 53−60.
(29) Cho, M.; Yu, J.-Y.; Joo, T.; Nagasawa, Y.; Passino, S. A.; Fleming, G. A. *J. Phys. Chem.* **1996**, *100*, 11944−11953.
(30) Jimenez, R.; Mourick, F. V.; Yu, J. Y.; Fleming, G. R. *J. Phys. Chem. B* **1997**, *101*, 7350−7359.
(31) Haley, M. M.; Langsdorf, B. L. *Chem. Commun.* **1997**, 1121−1122.
(32) Nagasawa, Y.; Watanabe, A.; Takikawa, H.; Okada, T. *J. Phys. Chem. A* **2003**, *107*, 632−641.
(33) Varnavski, O.; Sukhomlinova, L.; Twieg, R., Goodson, T. *J. Phys. Chem. B* **2004**, *108*, 10484−10492.
(34) Frisch, M. J.; Trucks, G. W.; Schlegel, H. B.; Scuseria, G. E.; Robb, M. A.; Cheeseman, J. R.; Montgomery, J. A., Jr.; Vreven, T.; Kudin, K. N.; Burant, J. C.; Millam, J. M.; Iyengar, S. S.; Tomasi, J.; Barone, V.; Mennucci, B.; Cossi, M.; Scalmani, G.; Rega, N.; Petersson, G. A.; Nakatsuji, H.; Hada, M.; Ehara, M.; Toyota, K.; Fukuda, R.; Hasegawa, J.; Ishida, M.; Nakajima, T.; Honda, Y.; Kitao, O.; Nakai, H.; Klene, M.; Li, X.; Knox, J. E.; Hratchian, H. P.; Cross, J. B.; Adamo, C.; Jaramillo, J.; Gomperts, R.; Stratmann, R. E.; Yazyev, O.; Austin, A. J.; Cammi, R.; Pomelli, C.; Ochterski, J. W.; Ayala, P. Y.; Morokuma, K.; Voth, G. A.; Salvador, P.; Dannenberg, J. J.; Zakrzewski, V. G.; Dapprich, S.; Daniels, A. D.; Strain, M. C.; Farkas, O.; Malick, D. K.; Rabuck, A. D.; Raghavachari, K.; Foresman, J. B.; Ortiz, J. V.; Cui, Q.; Baboul, A. G.; S. Clifford; Cioslowski, J.; Stefanov, B. B.; Liu, G.; Liashenko, A.; Piskorz, P.; Komaromi, I.; Martin, R. L.; Fox, D. J.; Keith, T.; Al-Laham, M. A.; Peng, C. Y.; Nanayakkara, A.; Challacombe, M.; Gill, P. M. W.; Johnson, B.; Chen, W.; Wong, M. W.; Gonzalez, C.; Pople, J. A. Gaussian 03, (Development version) Revision D.01; Gaussian Inc.: Wallingford, CT, 2004.
(35) Becke, A. D. *Phys. Rev. A* **1988**, *38*, 3098−3100.
(36) Becke, A. D. *J. Chem. Phys.* **1993**, *98*, 1372−1377.
(37) Foresman, J. B.; Head-Gordon, M.; Pople, J. A.; Frisch, M. J. *J. Phys. Chem.* **1992**, *96*, 135−149.
(38) Head-Gordon, M.; Rico, R. J.; Oumi, M.; Lee, T. J. *Chem. Phys. Lett* **1994**, *219*, 21−29.
(39) Head-Gordon, M.; Maurice, D.; Oumi, M. *Chem. Phys. Lett.* **1995**, *246*, 114−121.
(40) Bauernschmitt, R.; Ahlrichs, R. *Chem. Phys. Lett.* **1996**, *256*, 454−456.
(41) Casida, M. E.; Jamorski, C.; Casida, K. C.; Salahub, D. R. *J. Chem. Phys.* **1998**, *108*, 4439−4449.
(42) Stratmann, R. E.; Scuseria, G. E.; Frisch, M. J. *J. Chem. Phys.* **1998**, *109*, 8218−8224.
(43) McHale, J. L. *Molecular Spectroscopy*, 1st ed.; Prentice Hall: Upper Saddle River, NJ, 1999.
(44) Bernhardsson, A.; Forsberg, N.; Malmqvist, P.-A.; Roos, B. O.; Serrano-Andres, L. *J. Chem. Phys.* **2000**, *112*, 2798−2809.
(45) Kopelman, R.; Shortreed, M.; Shi, Z. Y.; Tan, W. H.; Xu, Z. F.; Moore, J. S.; BarHaim, A.; Klafter, J. *Phys. Rev. Lett.* **1997**, *78*, 1239−1242.
(46) Melinger, J. S.; Pan, Y.; Kleiman, V. D.; Peng, Z.; Davis, B. L.; McMorrow, D.; Lu, M. *J. Am. Chem. Soc.* **2002**, *124*, 12002−12012.
(47) Thompson, A. L.; Gaab, K. M.; Xu, J.; Bardeen, C. J.; Martinez, T. J. *J. Phys. Chem. A* **2004**, *108*, 671−682.
(48) Werner, H.-J.; Knowles, P. J. *J. Chem. Phys.* **1985**, *82*, 5053−5063.
(49) Knowles, P. J.; Werner, H.-J. *Chem. Phys. Lett.* **1985**, *115*, 259−267.
(50) Roos, B. O. *Adv. Chem. Phys.* **1987**, *69*, 399−455.
(51) Andersson, K.; Malmqvist, P.-A.; Roos, B. O.; Sadlej, A. J.; Wolinsji, K. *J. Phys. Chem.* **1990**, *94*, 5483−5488.
(52) Andersson, K.; Malmqvist, P.-A.; Roos, B. O. *J. Chem. Phys.* **1992**, *96*, 1218−1226.
(53) Celani, P.; Werner, H.-J. *J. Chem. Phys.* **2000**, *112*, 5546−5557.
(54) Stanton, J. F.; Bartlett, R. J. *J. Chem. Phys.* **1993**, *98*, 7029−7039.
(55) Hsu, C.-P.; Hirata, S.; Head-Gordon, M. *J. Phys. Chem. A* **2001**, *105*, 451−458.
(56) Cai, Z.-L.; Sendt, K.; Reimers, J. R. *J. Chem. Phys.* **2002**, *117*, 5543−5549.
(57) Dreuw, A.; Head-Gordon, M. *J. Am. Chem. Soc.* **2004**, *126*, 4007−4016.
(58) Matsuzawa, N. N.; Ishitani, A.; Dixon, D.; Uda, T. *J. Phys. Chem. A* **2001**, *105*, 4953−4962.
(59) Mukamel, S. *Principles of Nonlinear Optical Spectroscopy*; Oxford University Press: New York, 1995.
(60) Watanabe, J.; Hayasaka, T.; Nakahara, J. *J. Lumin.* **1996**, *66−67*, 55−60.
(61) Bardeen, C. J.; Cerullo, G.; Shank, C. V. *Chem. Phys. Lett.* **1997**, *280*, 127−133.
(62) Ohta, K.; Yang, M.; Fleming, G. R. *J. Chem. Phys.* **2001**, *115*, 7609−7621.
(63) Lee, J. H.; Min, C.; Joo, T. *J. Chem. Phys.* **2001**, *114*, 377−381.
(64) Harcourt, R. D.; Scholes, G. D.; Ghiggino, K. P. *J. Chem. Phys.* **1994**, *101*, 10521−10525.
(65) Scholes, G. D.; Harcourt, R. D.; Ghiggino, K. P. *J. Chem. Phys.* **1995**, *102*, 9574−9581.
(66) Scholes, G. D.; Harcourt, R. D. *J. Chem. Phys.* **1996**, *104*, 5054−5061.